Independently Tunable Dual-Band Perfect Absorption in a Dual-Resonance Hybrid Structure Incorporating Graphene

Shashi Zhang, Haixia Liu, Yongzhi Fang, Min Li, Hao Ding, and Lijun Zhao

***Abstract*—An independently tunable dual-resonance hybrid structure incorporating graphene is proposed to achieve selective light trapping and response tuning in the visible and near-infrared band. The incident light with different wavelengths are intensely localized in two separated resonant cavities via the synergetic effect of the guided mode resonances (GMRs) and optical Tamm states (OTSs), which leads to the strong enhancement of the light-matter interaction of graphene in different parts of the structure. The dual-band perfect absorption associated with critical coupling is achieved, whereas the two resonant modes can be independently tuned by adjusting the corresponding structural parameters. Furthermore, by dynamically changing the permittivity of the resonant cavities or the chemical potential of graphene, the absorption wavelength can be continuously adjusted and the absorption efficiency can be regulated stepwise.**

***Index Terms*—Graphene, dual-band, perfect absorption, active tunability, subwavelength structures, gratings.**

I. Introduction

OVER the past decade, graphene has broadly attracted attention in the field of opto-electronics owing to its ultra-high mobility and ultra-broad response band [1]. Particularly, the unique electrical tunability of graphene (i.e., the complex conductivity can be tuned by applying extra voltage [2]) also provides a novel way to develop the tunable optical devices. However, the weak single-pass absorption $A \approx 2.3\%$ [3]of the one-atom thick graphene severely limits its performance in the practical devices, especially in sensing, detection and radiation [4]. In frequency ranges from visible to near-infrared, considering the plasmonic response is absent for the undoped or unpatterned graphene [5], [6], various configurations based on the optical resonant modes have been proposed to enhance the light-matter interactions, including Fabry–Perot(FP) cavity modes [7], photonic crystal(Phc) defective modes [8],optical Tamm states (OTSs) [9] and guided mode resonances (GMRs) [10].

Conventionally, one single resonant mode usually provides only one channel, meaning that the light-matter interaction is enhanced in a particular wavelength. However, dual or more channels may be desired in some applications, including multi-band detectors [11], solar cells [12] and white light emitting devices [13]. For this case, some hybrid systems with multiple resonant modes have been proposed. Qing *et al.* [14] achieved tunable dual-band perfect absorption in a composite structure consists of a graphene ribbon array and a distributed Bragg reflector. Cai *et al.* [15] implemented a dual-band graphene-based absorber combining the magnetic resonance with a cold mirror. Long [16] achieved multi-channel ultranarrow absorption by employing a subwavelength dielectric grating to excite multi-order guided-mode resonances. Nevertheless, most of these works conduct with the same monolayer of graphene as the active medium, without considering the independent extraction of dual-band signals. Meanwhile, due to the proximity or overlap of the excitation components, the hybridization effect [17] of the dual modes prevents independent adjustment of the dual-band absorption response. In addition, designs that deposit graphene on the surface of the device may lead to damage to integrity and stability of the graphene layer during practical processing, resulting in additional loss channels [18].

In this paper, we propose an independently tunable dual-resonance hybrid structure to achieve selective light trapping and response tuning in the visible and near-infrared band. The duplex real-time operation is ensured by exciting GMRs and OTSs in two separated resonant cavities containing graphene, which leads to the dual-band perfect absorption with a promising subregional absorption effect. Incorporating the different physical mechanisms of the resonant states, the dual-band absorption response can be independently modulated via changing the corresponding structural parameters. More importantly, by changing the permittivity of the resonant cavities or the chemical potential of graphene, the dynamic tunability can be achieved, whereas the absorption wavelength can be continuously adjusted and the absorption efficiency can be regulated stepwise. A comparison of some recent reported graphene-based dual-band absorber is presented. Finally, the fabrication of the proposed structure is studied in the context of recent developments, which is expected to solve the technical challenges of embedding

Manuscript received August 7, 2021; revised September 26, 2021; accepted October 6, 2021. Date of publication October 11, 2021; date of current version November 2, 2021. This work was supported by the China CAST Innovation under Grant CAST-BISEE2019-027. *(Corresponding author: Haixia Liu.)*

Shashi Zhang is with the School of Instrumentation and Optoelectronic Engineering, Beihang University, Beijing 100191, China, and also with the Peoples Liberation Army Engineering University, Xuzhou 221000, China (e-mail: 467665905@qq.com).

Haixia Liu and Hao Ding are with the School of Instrumentation and Optoelectronic Engineering, Beihang University, Beijing 100191, China (e-mail: liuhx08@buaa.edu.cn; 346103590@qq.com).

Yongzhi Fang, Min Li, and Lijun Zhao are with the Peoples Liberation Army Engineering University, Xuzhou 221000, China (e-mail: 1278121796@qq.com; 13842034092@163.com; 1042765636@qq.com).

Digital Object Identifier 10.1109/JPHOT.2021.3119021

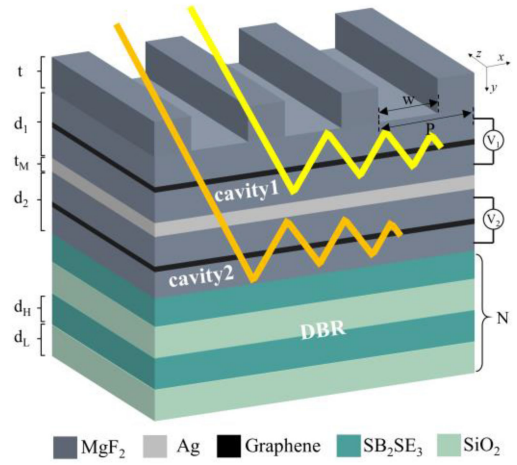

Fig. 1. Schematic diagram of the dual-resonance hybrid structure consisting of a dielectric grating, a silver film, a distributed Bragg reflector (DBR) and two resonant cavities (labeled as cavity1 and cavity2). The chemical potential μ_c of graphene1 and graphene2 can be independently regulated by the voltages V_1 and V_2.

monolayer graphene in the dielectric cavity and pave the way for the large-scale preparation of devices for applications.

II. Design And Methods

The schematic diagram of the proposed structure is shown in Fig. 1, which consists of a dielectric grating, a silver film, a distributed Bragg reflector (DBR) and two resonant cavities (labeled as cavity1 and cavity2) with permittivity of ε_1, ε_2 and thickness of d_1, d_2, respectively. Graphene1 and graphene2 are inserted in the middle of cavity 1 and cavity 2, which are deposited on both sides of the silver film. When light is incident from the top, the GMRs and OTSs excited by the top grating and the bottom DBR would localize the optical field in cavity1 and cavity2, forcing it to interact with the graphene inserted. The chemical potential μ_c of graphene1 and graphene2 can be adjusted independently by the gate voltage V_1 and V_2. The top grating made of MgF_2 can be described by parameters consisting of period P, height t and ridge width w, whereas the bottom DBR is made up of N pairs of SB_2SE_3/SiO_2 dielectric layers, with the thickness of d_H and d_L, respectively. Since the bottom DBR is able to induce a wide enough forbidden band in the operating range, all transmissions are blocked, making the entire structure a single-port system. Thus, the system absorption can be expressed as $A = 1\text{-}R$.

To improve the accuracy of the numerical analysis, the simulations are performed using both of coupled-wave analysis (RCWA) method and the finite element method (FEM). The reflection and absorption can be obtained by accumulating the forward and reverse diffraction efficiencies of the system [30] by means of RCWA, whereas the FEM can be applied to resolve the distribution of the internal optical field and power dissipation density by setting one period unit as the simulation domain. In simulation, TE-polarized plane wave (electric field parallel to the z-axis) irradiates the hybrid structure along the positive direction of x-axis normally (incident angle $\theta = 0$). All metals are modeled

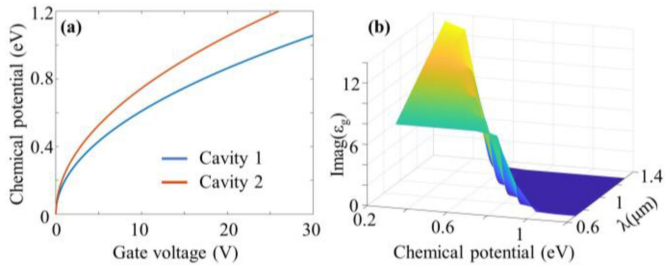

Fig. 2. (a) Dependence of the chemical potential μ_c on the gate voltage applied for cavity 1 and cavity 2. (b) imaginary parts of graphene permittivity ε_g versus different chemical potential and wavelengths.

as a dispersive silver using Drude model [19]. The graphene layer can be modeled as an ultrathin layer with certain thickness $t_g = 0.334nm$ and the permittivity of $\varepsilon_g = 1 - i\sigma_s/(\omega\varepsilon_o t_g)$, where ω is the angular frequency of the incident light, ε_0 is the vacuum dielectric constant. σ_S is the graphene surface conductivity, which can be obtained from the Kubo equation [20]:

$$\sigma_s = i\frac{e^2 k_B T}{\pi\hbar(\omega + i\tau^{-1})}\left[\frac{\mu_c}{k_B T} + 2\ln\left(\exp\left(-\frac{\mu_c}{k_B T}\right) + 1\right)\right] + i\frac{e^2}{4\pi\hbar}\ln\left[\frac{2|\mu_c| - \hbar(\omega + i\tau^{-1})}{2|\mu_c| + \hbar(\omega + i\tau^{-1})}\right] \quad (1)$$

Here, k_B, T, e and $\bar{h}$ represent the Boltzmann constant, Kelvin temperature, electron charge and reduced Planck's constant, respectively.$\tau = \mu\mu_c/ev_F^2$ is the momentum relaxation time, where $v_F = 10^6 m/s$ and$\mu = 10^4 cm^2/(V \cdot s)$. $\mu_c = \hbar v_F\sqrt{\pi n_s}$ is the chemical potential of graphene being as a function of carrier density n_s, whereas $n = \varepsilon_d\varepsilon_0 V_g/ed_n$ is in turn proportional to the gate voltage V_g applied to the graphene layer,ε_d and d_n are the relative permittivity and thickness of the dielectric layer (i.e., cavity 1 and cavity 2), respectively. Thus, the relationship between μ_c and V_g can be obtained as $\mu_c = \hbar v_F\sqrt{\pi\varepsilon_d\varepsilon_0 V_g/ed}$, which is shown in Fig 2(a). Since the absorption properties of graphene is mainly related to the imaginary part of its permittivity (Imag(ε_g)), we further present Imag(ε_g) as a function of the chemical potential μ_c over a range from 0.7 to 1.3μm in Fig. 2(b), which clearly indicates that Im(ε_g) corresponding to different wavelengths decreases stepwise at certain μ_c values, leading to a direct weakening of the graphene light absorption.

III. Results And Discussion

We set the basic structural and optical parameters of the structure as follows: $P = 0.69\,\mu m, t = 0.2\,\mu m, w = 0.35\,\mu m, d_1 = 0.17\,\mu m,\ d_2 = 0.341\,\mu m,\ d_H = 0.058\,\mu m,\ d_L = 0.164\,\mu m,$ $t_M = 31nm, N = 6$ and $\varepsilon_1 = \varepsilon_2$=1.37. The chemical potential μ_c of graphene is chosen as 0.3eV (V_1 = 2.4V, V_2 = 1.7V). All materials' datas are taken from [21]. The absorption spectra of the proposed structure using RCWA is given in Fig. 3(a), whereas the two narrow-band resonant peaks can be found at 0.753 μm and 1.176 μm (labeled as Mode1 and Mode2),

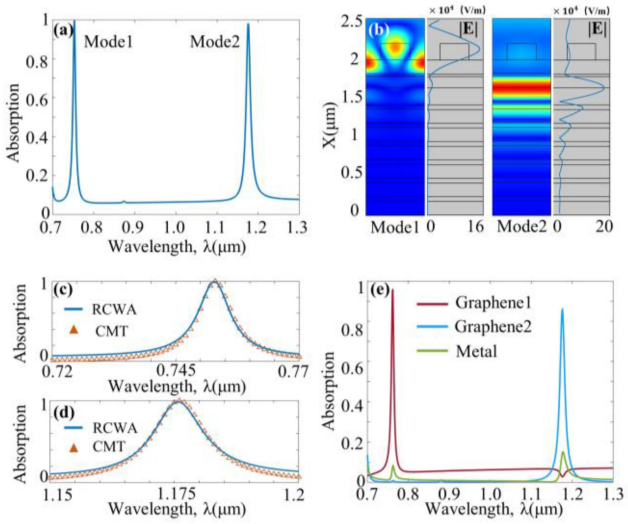

Fig. 3. (a) RCWA calculation results of the absorption spectra for TE polarization. Two narrow-band resonant peaks can be found at 0.753 μm and 1.176 μm (labeled as Mode1 and Mode2), with absorption reaching 99.53% and 98.08% respectively. (b) Profile of electric field magnitude and amplitude distribution of Mode1 and Mode2. (c) RCWA calculated and CMT fitted spectral absorptance of Mode1. (d) RCWA calculated and CMT fitted spectral absorptance of Mode2. (e) Absorption contribution of the lossy medium to the absorption response from area fraction of the power dissipation density in the x-z planes.

with absorption reaching 99.53% and 98.08%, respectively. The physical origin of two resonant peaks can be analyzed through the field distribution shown in Fig. 3(b). For case of Mode1, the optical field is almost confined within the cavity1 with a standing-wave pattern in *y*-direction, which coincides with the typical characteristics of GMRs [22]. For case of Mode2, the most incident electromagnetic energy is trapped in cavity2 between the DBR and the silver film owing to the excitation of OTSs. This indicates that The dual-band perfect absorption is mainly attributed to the critical coupling properties of two resonant modes, whereas the graphene inserted in cavities as the dissipative layers can effectively absorb the incident light in spite of its one-atom thickness.

Furthermore, the critical coupling induced by GMRs and OTSs can be illustrated by the coupled mode theory (CMT) [23], in which the spectral characteristics of the single-port structure with lossy medium loaded can be analytically interpreted [24]. The time domain evolution equation of the two resonant modes with each resonant frequency at ω_i is governed by [14]:

$$\frac{da_i}{dt} = (i\omega_i - \gamma_i - \delta_i)\, a_i + \sqrt{2\gamma_i} s_+ \tag{2}$$

$$s_- = s_+ - j\sqrt{2\gamma_i} a_i \tag{3}$$

where a_i denotes the normalized amplitude of resonant mode, ω_i denotes the resonant frequency, s_+ and s_- represent the amplitudes of system input and output wave. Combining (2) and (3), the absorption of the system can be solved as:

$$A(\omega) = 1 - |r(\omega)|^2 = \frac{4\delta_i \gamma_i}{(\omega - \omega_i)^2 + (\delta_i + \gamma_i)^2} \tag{4}$$

Here, δ and γ_e is the intrinsic loss rate and external leakage rate, respectively. At the resonant frequency ω_i, only when the external leakage rate is equal to the intrinsic loss (i.e., δ=γ_e), the critical coupling occurs and the incident energy can be fully captured and absorbed. By fitting the absorption spectra of Mode1, the fitted $\delta_1 = \gamma_1 = 6.9132 \times 10^{12} Hz$ is obtained. The absorption spectra calculated by inputting the values into (4) give a comparison with the results from the RCWA, which is shown in Fig. 3(c). The great agreement between CMT model and RCWA method indicates that CMT can provide a proper interpretation for the system in the vicinity of the resonance. The deviation of CMT and RCWA in the region away from resonance is due to the theoretical assumption in which the loss away from resonance is 0 [25]. Similarly, for Mode2, the fitted $\delta_2 = \gamma_2 = 4.4266 \times 10^{12} Hz$ is also obtained. The absorption spectra calculated by CMT for Mode2 is shown in Fig. 3(d), which indicates that the absorption peak at 1.176μm can be attributed to the critical coupling with OTSs mode.

To further investigate the subregional absorption effect of the hybrid structure, we calculated the absorption contribution of the lossy materials (i.e., graphene and silver) from the area fraction of power dissipation density in the *x*-*z* plane, which can be determined by the formula [26]:

$$w(x,z) = \frac{1}{2} c_0 \omega \mathrm{Im}(\varepsilon(x,z)) |E(x,z)|^2 \tag{5}$$

Here, $\varepsilon(x,z)$ is the imaginary part of the relative dielectric constant of the lossy material, $E(x,z)$ is the spatially distributed electric field in the *x*-*y* plane. The calculated results are depicted in Fig. 3(e). For mode1 at 0.753μm, the absorption contribution of graphene 1 reaches 91.21%, while only 8.79% derives from the silver film and graphene2. Conversely, for mode2 at 1.176μm, the absorption contribution of graphene 2 reaches 85.94%, while only 14.06% derives from the other parts. This kind of absorption distribution provides great convenience for independent extraction of dual-channel signals.

Since the physical mechanisms and excitation components of the two resonant modes are completely different, we further explored the absorption response dependence on the structural parameters. Firstly, for Mode1, it can be indicated from Fig. 4(a) that the resonant wavelength of Mode1 possesses an obvious redshift with the increase of grating period *P*, and a high absorption (>97%) is obtained in the range of 0.72μm-0.777μm, while Mode2 remains basically unchanged. This is consistent with the excitation conditions of GMR, whereas the resonance wavelength is a linear function of the grating period [27]. As shown in Fig. 4(b), the resonant wavelength of Mode2 experiences a slightly blueshift with the increase of the silver film thickness t_M, while Mode1 is almost unaffected. The trace shift of Mode2 is due to the variation of the amplitude reflection coefficient of the silver film when its thickness changes, which leads to additional phase shift of light propagation in cavity2. Further, since the incident electromagnetic energy is mostly trapped in two cavities, the properties of the resonant cavities have a dramatic influence on the absorption response. The dependence of absorption on the cavity1 thickness d_1 is shown in Fig. 4(c), which indicates that the multi-band absorption can be achieved with the periodic

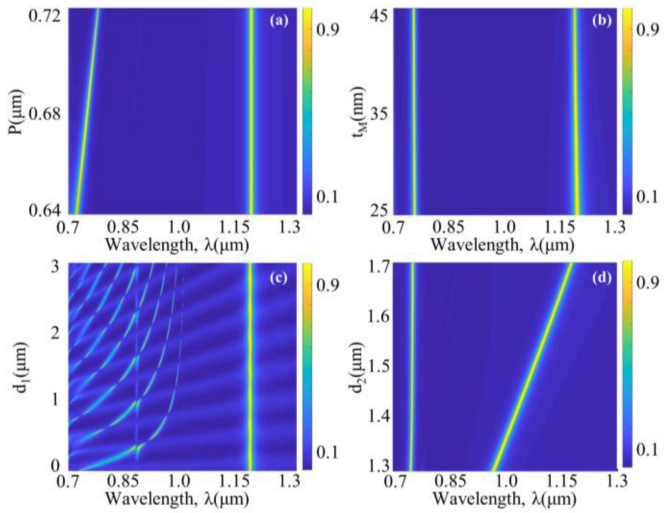

Fig. 4. (a) Absorption maps by RCWA as a function of the grating period P. (b) Absorption spectra dependence on the number of the silver film thickness t_M. (c) Absorption response by RCWA with respect to the cavity1 thickness d_1. (d) Absorption response by RCWA with respect to cavity2 thickness d_2.

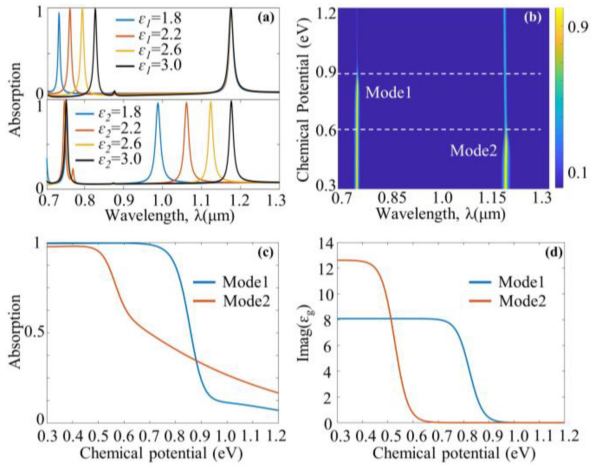

Fig. 5. (a) Absorptance spectra of the hybrid structure with different dielectric permittivities. (b) Absorption response as a function of chemical potential μc of graphene1 and graphene2. (c) Absorption spectra as a function of the chemical potential μ_c at 761nm and 1176nm, wherein the chemical potential of the entire graphene sheet is assumed to change with the gate voltage simultaneously. (d) Imaginary parts of the permittivity of graphene versus different chemical potential.

maxima distance, owing to the excitation of the higher-order resonant modes of GMRs when d_1 increases [28]. As shown in Fig. 4(d), the resonant wavelength of Mode2 undergoes a significant redshift with the increase of the cavity2 thickness d_2 in a wide range from 0.968μm to 1.176μm, whereas Mode1 is almost unaffected. When mode 2 is reflected back and forth between the silver film and the DBR, the phase condition can be described asφ=$\varphi_{metal} + \varphi_{DBR} + 2\pi d_2/\lambda_{OTS} n_2 = 2m\pi$. As d_2 increases, the resonant wavelengthλ_{OTS} of mode2 must also increase accordingly to maintain the equation when other conditions remain unchanged. Therefore, the cavity2 thickness d_2 can be considered as the main modulation parameter for the resonant wavelength of mode2.

It is worth noting that the absorption tuning via the structural parameters is no longer available once fabricated. Therefore, we continued to investigate the dynamic modulating mechanism of the absorption wavelength and the absorption efficiency, which is based on the variation of the cavity permittivity and the graphene chemical potential μ_c, respectively. The absorption spectra of mode1 and mode2 with different permittivities is shown in Fig. 5(a). We introduce the figure of merit (FOM) [29] to evaluate the modulation sensitivity of the absorption wavelength, which can be expressed by $FOM = \Delta\lambda/FWHM$, $\Delta\lambda$ and $FWHM$are the absorption wavelength offset and the full width at half maximum. When the permittivity of the cavity increases from 1.8 to 3, the absorption wavelengths of both modes possess a significant redshift and FOM reaches 8.5 and 14.46, while the high absorption (>96%) maintains. At the same time, the variation of the permittivity of one resonant cavity has no effect on the other one. This indicates that the independent modulation of the absorption wavelengths can be achieved via selecting the suitable permittivity for each of the two cavities. Further, in order to realize the dynamic tunability of the absorption wavelengths, the organic optoelectronic materials such as liquid crystals [30] can be used for two resonant cavities, and additional voltages can be applied as needed for practical purposes.

Meanwhile, since graphene makes the major contribution to the light absorption, we further explored the dynamic regulation of absorption efficiency based on the variation of the chemical potential μ_c of graphene. The absorption response as a function of chemical potential μ_c is shown in Fig. 5(b). For Mode1, as μ_c increases, the absorption efficiency exhibits a step break at 0.85eV (corresponding to $V_1 = 19.4$V), whereas the absorption wavelength is almost unaffected. The same trend is seen in Mode2, in which the step point is located at 0.58eV ($V_2 = 6.1$V). We introduced the modulation depth (MD) to further investigate the absorption efficiency modulation properties, which can be expressed as $MD = (A_0 - A_M)/A_0$, A_0 and A_M are the absorption efficiency before and after modulation. As shown in Fig. 5(c), when μ_c increases from 0.3eV ($V_1 = 2.4$V, $V_2 = 1.7$V) to 1.2eV ($V_1 = 37.9$V, $V_2 = 26$V), the absorption of Mode1 and Mode2 decrease from 99.53% to 5.45% and from 98.08% to 13.33%, whereas MD reaches 94.52% and 86.4%, respectively. To explain the cause of the dramatic decrease of absorption, we investigated the dependence of the imaginary part of ε_g (which is highly correlated with its loss characteristics) on the chemical potential μ_c. It can be inferred from Fig. 5(d) that graphene gradually converts from a lossy material to a lossless dielectric (Imag(ε_g) = 0) as μ_c increases, whereas the step point of the imaginary part of ε_g is in good agreement with that of the absorption. Meanwhile, a comparison of the performance of this work and some recently reported graphene-based dual-band absorbers is summarized in Table I, which indicates that the proposed structure not only possesses significant independent tuning characteristics, but also shows significant merits in terms of modulation sensitivity and modulation depth.

TABLE I
A COMPARISON OF SOME RECENT REPORTED GRAPHENE-BASED DUAL-BAND ABSORBERS

REF	FOM	MODULATION DEEPTH	INDEPENDENT TUNABILITY
[15]	13.78/6.13	14.18% / 15.79%	Unable
[14]	5.2/1.75	29.65% / 0.69%	Unable
[37]	19.1/20.2	9.5% / 2.9%	Unable
[38]	3.79/4.4	93.57% / 93.56%	Unable
This work	8.5/14.46	94.08% / 84.75%	Able

Lastly, the fabrication process of the proposed structure is studied in the line with recent developments of processing technology. The large-scale preparation of inorganic DBR stacked structures can be performed by chemical vapor deposition(CVD) [31], electron-beam evaporation [32], molecular beam epitaxy and sputtering [33]. However, when embedding monolayer graphene(MLG) inside a dielectric resonant cavity, disorder or oxidation caused by the sputtering process may destroy the integrity of MLG [34]. Nematpour *et al.* [35] successfully reduced sputtering induced damage by evaporating a thin MgF_2 layer on MLG by means of CVD, which coincides with the material used in this paper. Therefore, in the initial preparation stage of proposed structure, the bottom DBR can be sputtering first and used as a substrate to transfer MLG by wet transfer method [36]. Then, evaporating the MgF_2 layer on top of MLG using CVD technology to form a resonant cavity, on which the top dielectric layers can be sputtered continuously. Finally, the top gratings can be etched using high-throughput and low-cost laser interference lithography or nanoimprint lithography [22]. This fabrication process is expected to solve the technical challenges of embedding MLG in the dielectric cavity and pave the way for the large-scale preparation of devices for applications.

IV. CONCLUSION

In this paper, we proposed an independently tunable dual-resonance hybrid structure achieve selective light trapping and absorbing in the visible and near-infrared band. The strong optical field localization induced by the excitation of GMRs and OTSs in two resonant cavities greatly enhance the light-interaction of graphene, which provides great convenience for independent extraction of dual-channel signals and the opportunity for the independent modulation of two resonant peaks. Numerical results indicated that the two resonant peaks can be independently modulated via the variation of corresponding geometrical parameters over a range about 100nm. Meanwhile, the dynamic modulating mechanism of the absorption response can be achieved via the active variation of the cavity permittivity and the graphene chemical potential. The feasibility of the large-scale preparation of the proposed structure is studied as well. This work can serve as a dynamic building block for the graphene-based multichannel optical systems and provide useful reference for related fields, including detection, sensing, switches and filters.

REFERENCES

[1] K. S. Kim *et al.*, "Large-scale pattern growth of graphene films for stretchable transparent electrodes," *Nature*, vol. 457, no. 7230, pp. 706–710, Feb. 2009.

[2] L. Ye, K. Sui, Y. Zhang, and Q. H. Liu, "Broadband optical waveguide modulators based on strongly coupled hybrid graphene and metal nanoribbons for near-infrared applications," *Nanoscale*, vol. 11, no. 7, pp. 3229–3239, Feb. 2019.

[3] R. R. Nair *et al.*, "Fine structure constant defines visual transparency of graphene," *Science*, vol. 320, no. 5881, Jun. 2008, Art. no. 1308.

[4] J. Wang, L. Yang, Z.-D. Hu, W. He, and G. Zheng, "Analysis of graphene-based multilayer comb-like absorption system based on multiple waveguide theory," *IEEE Photon. Technol. Lett.*, vol. 31, no. 7, pp. 561–564, Apr. 2019.

[5] L. Ye, K. Sui, and H. Feng, "High-efficiency couplers for graphene surface plasmon polaritons in the mid-infrared region," *Opt. Lett.*, vol. 45, no. 2, pp. 264–267, Jan. 2020.

[6] F. Xia, H. Yan, and P. Avouris, "The interaction of light and graphene: Basics, devices, and applications," *Proc. IEEE*, vol. 101, no. 7, SI, pp. 1717–1731, Jul. 2013.

[7] C. Handschin *et al.*, "Fabry-Perot resonances in a Graphene/hBN moire superlattice," *Nano Lett.,* vol. 17, no. 1, pp. 328–333, 2017.

[8] M. Grande *et al.*, "Absorption and losses in one-dimensional photonic-crystal-based absorbers incorporating graphene," *IEEE Photon. J.,* vol. 6, no. 6, Dec. 2014, Art. no. 0600808.

[9] K. Zhou, L. Lu, J. Song, B. Li, and Q. Cheng, "Ultra-narrow-band and highly efficient near-infrared absorption of a graphene-based Tamm plasmon polaritons structure," *J. Appl. Phys.*, vol. 124, no. 12, Sep. 2018, Art. no. 123102.

[10] D. de Ceglia *et al.*, "Tuning infrared guided-mode resonances with graphene," *J. Opt. Soc. Amer. B-Opt. Phys.*, vol. 33, no. 3, pp. 426–433, Mar. 2016.

[11] B. Zhang, Q. Cui, M. Piao, and Y. Hu, "Design of dual-band infrared zoom lens with multilayer diffractive optical elements," *Appl. Opt.*, vol. 58, no. 8, pp. 2058–2067, Mar. 2019.

[12] W. R. Erwin, H. F. Zarick, E. M. Talbert, and R. Bardhan, "Light trapping in mesoporous solar cells with plasmonic nanostructures," *Energy Environ. Sci.*, vol. 9, no. 5, pp. 1577–1601, 2016.

[13] Y.-F. Liu *et al.*, "Omnidirectional emission from top-emitting organic light-emitting devices with microstructured cavity," *Opt. Lett.*, vol. 37, no. 2, pp. 124–126, Jan. 2012.

[14] Y. M. Qing, H. F. Ma, S. Yu, and T. J. Cui, "Tunable dual-band perfect metamaterial absorber based on a graphene-SiC hybrid system by multiple resonance modes," *J. Phys. Appl. Phys.*, vol. 52, no. 1, Jan. 2019, Art. no. 015104.

[15] Y. Cai, Y. Guo, Y. Zhou, X. Huang, G. Yang, and J. Zhu, "Tunable dual-band terahertz absorber with all-dielectric configuration based on graphene," *Opt. Exp.*, vol. 28, no. 21, pp. 31524–31534, Oct. 2020.

[16] L.-A. Bian, L. Yang, P. Liu, Y. Chen, H. Liu, and Q. Zhou, "Controllable perfect absorption in a double-cavity photonic crystal with one graphene monolayer," *J. Phys. Appl. Phys.*, vol. 51, no. 2, Jan. 2018, Art. no. 025106.

[17] J. Nong *et al.*, "Strong coherent coupling between graphene surface plasmons and anisotropic black phosphorus localized surface plasmons," *Opt. Exp.*, vol. 26, no. 2, pp. 1633–1644, Jan. 2018.

[18] J. Nie and H.-Q. Li, "Ultranarrowband perfect terahertz absorber based on a metal- and insulator-stacked structure," *J. Opt. Soc. Amer. B-Opt. Phys.*, vol. 33, no. 12, pp. 2602–2608, Dec. 2016.

[19] L. Ye, F. Zeng, Y. Zhang, and Q. H. Liu, "Composite graphene-metal microstructures for enhanced multiband absorption covering the entire terahertz range," *Carbon*, vol. 148, pp. 317–325, 2019.

[20] G. W. Hanson, "Dyadic green's functions and guided surface waves for a surface conductivity model of graphene," *J. Appl. Phys.*, vol. 103, no. 6, Mar. 2008, Art. no. 064302.

[21] A. Addamiano *et al.*, "Handbook of optical constants of solids," *Opt. Acta Int. J. Opt.*, vol. 39, no. 1, pp. 189–189, 1997.

[22] Y. Zhao, J. Lu, Y. Huo, B. Man, and T. Ning, "Enhanced third harmonic generation from graphene embedded in dielectric resonant waveguide gratings," *Opt. Commun.*, vol. 447, pp. 30–35, Sep. 2019.

[23] W. Suh, Z. Wang, and S. H. Fan, "Temporal coupled-mode theory and the presence of non-orthogonal modes in lossless multimode cavities," *IEEE J. Quantum Electron.*, vol. 40, no. 10, pp. 1511–1518, Oct. 2004.

[24] F. Liu, L. Chen, Q. Guo, J. Chen, X. Zhao, and W. Shi, "Enhanced graphene absorption and linewidth sharpening enabled by Fano-like geometric resonance at near-infrared wavelengths," *Opt. Exp.*, vol. 23, no. 16, pp. 21097–21106, Aug. 2015.

[25] J. R. Piper and S. Fan, "Total absorption in a graphene mono layer in the optical regime by critical coupling with a photonic crystal guided resonance," *Acs Photon.*, vol. 1, no. 4, pp. 347–353, Apr. 2014.
[26] B. Zhao, J. M. Zhao, and Z. M. Zhang, "Resonance enhanced absorption in a graphene monolayer using deep metal gratings," *J. Opt. Soc. Amer. B-Opt. Phys.*, vol. 32, no. 6, pp. 1176–1185, Jun. 2015.
[27] M. Grande *et al.*, "Graphene-based perfect optical absorbers harnessing guided mode resonances," *Opt. Exp.*, vol. 23, no. 16, pp. 21032–21042, Aug. 2015.
[28] M. Grande *et al.*, "Graphene-based absorber exploiting guided mode resonances in one-dimensional gratings," *Opt. Exp.*, vol. 22, no. 25, pp. 31511–31519, Dec. 2014.
[29] A.-K. U. Michel *et al.*, "Using low-loss phase-change materials for mid-infrared antenna resonance tuning," *Nano Lett.,* vol. 13, no. 8, pp. 3470–3475, 2013.
[30] G. Isic, B. Vasic, D. C. Zografopoulos, R. Beccherelli, and R. Gajic, "Electrically tunable critically coupled terahertz metamaterial absorber based on nematic liquid crystals," *Phys. Rev. Appl.*, vol. 3, no. 6, Jun. 2015, Art. no. 064007.
[31] S. T. Tan *et al.*, "Blueshift of optical band gap in ZnO thin films grown by metal-organic chemical-vapor deposition," *J. Appl. Phys.*, vol. 98, no. 1, 2005, Art. no. 1897.
[32] S. F. Chichibu, T. Ohmori, N. Shibata, and T. Koyama, "Dielectric SiO_2/ZrO_2 distributed Bragg reflectors for ZnO microcavities prepared by the reactive helicon-wave-excited-plasma sputtering method," *Appl. Phys. Lett.*, vol. 88, no. 16, pp. 3314, 2006.
[33] L. Paola, M. Giovanni, and C. Davide, "Advances in functional solution processed planar 1D photonic crystals," *Adv. Opt. Mater.*, vol. 6, no. 24, 2018, Art. no. 1800730.
[34] F. Johansson, P. Ahlberg, U. Jansson, S. L. Zhang, A. Lindblad, and T. Nyberg, "Minimizing sputter-induced damage during deposition of WS2 onto graphene," *Appl. Phys. Lett.*, vol. 110, no. 9, pp. 4598–4129, 2017.
[35] N. Abedin, L. Nicola, P. Angela, L. Laura, Guohang, and Maria, "Experimental near infrared absorption enhancement of graphene layers in an optical resonant cavity," *Nanotechnology*, vol. 30, no. 44, pp. 445201–445201, 2019.
[36] A. Capasso *et al.*, "Cyclododecane as support material for clean and facile transfer of large-area few-layer graphene," *Appl. Phys. Lett.*, vol. 105, no. 11, pp. 1312, 2014.
[37] K. Zhou, Q. Cheng, L. Lu, B. Li, J. Song, and Z. Luo, "Dual-band tunable narrowband near-infrared light trapping control based on a hybrid grating-based fabry-perot structure," *Opt. Exp.*, vol. 28, no. 2, pp. 1647–1656, Jan. 2020.
[38] G. C. Park and K. Park, "Tunable dual-wavelength absorption switch with graphene based on an asymmetric guided-mode resonance structure," *Opt. Exp.*, vol. 29, no. 5, pp. 7307–7320, Mar. 2021.